

High-energy polarized electron beams from the ionization of isolated spin polarized hydrogen atoms.

Dimitris Sofikitis^{1,*}, Marios G. Stamatakis², Dimitrios G. Papazoglou^{3,4}, and T. Peter Rakitzis^{3,5}

¹*Department of Physics, Atomic and Molecular Physics Laboratory,*

University of Ioannina, University Campus, Ioannina, GR-45110, Greece

²*Department of Mathematics, University Campus, Ioannina, GR-45110, Greece*

³*Institute of Electronic Structure and Lasers, Foundation for Research and Technology-Hellas, 71110 Heraklion-Crete, Greece.*

⁴*Materials Science and Technology Department, University of Crete, GR 70013, Heraklion, Greece and*

⁵*Department of Physics, University of Crete, 70013 Heraklion-Crete, Greece.*

(Dated: March 12, 2024)

We propose a laser-based method for the preparation of high-energy, highly-polarized electrons, from the ionization of isolated spin-polarized hydrogen (SPH) atoms. The SPH atoms are prepared from the photodissociation of HBr, using two consecutive shaped UV pulses of ps duration. By appropriately timing and focusing the pulses, we can spatially separate the highly polarized SPH from other unwanted photoproducts, which then act as the target for the ion-acceleration lasers. The density of SPH can surpass $\approx 10^{18} \text{ cm}^{-3}$, allowing the production of GeV electrons with polarization larger than 90%.

PACS numbers:

Polarized electron and positron beams are powerful experimental tools, used in a diverse set of disciplines ranging from studies of atomic and molecular structure [1, 2] and material science [3, 4], to nuclear and high energy physics [5], where electrons accelerated to relativistic energies can be used to test new physics beyond the standard model [6–8]. Producing intense beams of highly polarized, high-energy electrons can be done using conventional acceleration methods involving accumulation in storage rings [9, 10] as well as emerging methods involving filtering of polarized electrons [11, 12]. Alternatively, high-energy polarized electrons can be produced using polarized photocathodes [13, 14] or through laser ionization of noble gases [15, 16].

Laser wakefield acceleration of electrons [17], combined with recent laser methods for the preparation of high-density SPH [18–20], open a new potentiality: that of accelerating electrons resulting from the ionization of pre-polarized targets. Following this, a variety of recent proposals predict the production of GeV spin-polarized electron beams utilizing such targets [21–24].

The direct use, however, of such SPH atoms as targets for electron acceleration is limited by several factors. The presence of the halide atoms means that their valence electrons (which are only weakly polarized by the photodissociation) and inner-shell electrons (which are unpolarized) are also liberated and accelerated, lowering the total polarization of the accelerated electrons to very low values. It is possible to ionize the halide atom and subsequently remove the ions using electric fields [24], however, this is quite challenging to achieve within the timescales required for laser acceleration. Additionally, the SPH polarization depends on the parent molecule bond orientation, resulting in a $\cos^2\theta$ spatial distribution of the polarization, a fact that sets an upper limit for the free-space value for polarization of 40%. Bond orientation, which

can lift this limitation, can be achieved using a strong IR pulse. However, apart from the complication of using an extra pulse of different wavelength, bond alignment cannot be 100% successful for moderate IR pulse intensities needed to avoid unwanted multi-photon or even field ionization effects. Finally, the hyperfine structure of hydrogen atoms causes the polarization to oscillate from the electron to the proton and backwards, with a period of 0.7 ns, meaning that any manipulation aimed to removing the unwanted halide atoms or to achieving bond orientation, has to be completed within this time to avoid further reduction of electron polarization. Proposed solutions lead to experimental complications, ultimately limiting the method’s feasibility.

Here, we propose a simple and intuitive method which circumvents all the limitations mentioned above. The method takes advantage the kinematics of the dissociation process, the angular distribution of the polarization of the atomic fragments and the shape of the dissociation laser beams, to produce pure samples of highly polarized SPH, without the presence of the unwanted halide partners. In the first step, we illuminate an HBr sample using a tightly focused laser to dissociate all molecules in a volume around the focus. The Br and H atomic fragments will acquire large velocities, that will cause them to exit the laser focus within a few tens of ns, creating a volume devoid of atoms or molecules, hereafter referred to as ‘hole’. In the second step, a second dissociation pulse of larger spatial dimensions (but of same wavelength and pulse duration as the first), dissociates molecules in a larger volume around the hole, hereafter called the ‘reservoir’. Now, SPH atoms will fly from the reservoir to the hole volume (much faster than the heavier Br atoms), where they can be ionized to produce accelerated electrons by a an ionization-acceleration pulse in the third step. The narrow velocity distributions of the fragments

and the available dissociation laser beam geometries, allow tailoring the hole and reservoir geometries, so that in the third step, only hydrogen atoms of high polarization ($P \gtrsim 90\%$) are contained inside the hole.

We consider Dissociation Pulses 1 (DP1) and 2 (DP2), of the same wavelength and duration (213 nm and a few ps for example), but with different spotsize, intensity and synchronization. The pulses are directed towards a molecular beam containing HBr molecules at a temperature of few K (Fig.1). The molecular beam moves with a velocity around 1000 m/s perpendicular to the direction of propagation of the dissociation pulses; for simplicity, let us use the reference frame of the moving molecular beam.

At $t = 0$, the pulse DP1 will dissociate all HBr molecules in the volume of the hole, which is shaped as

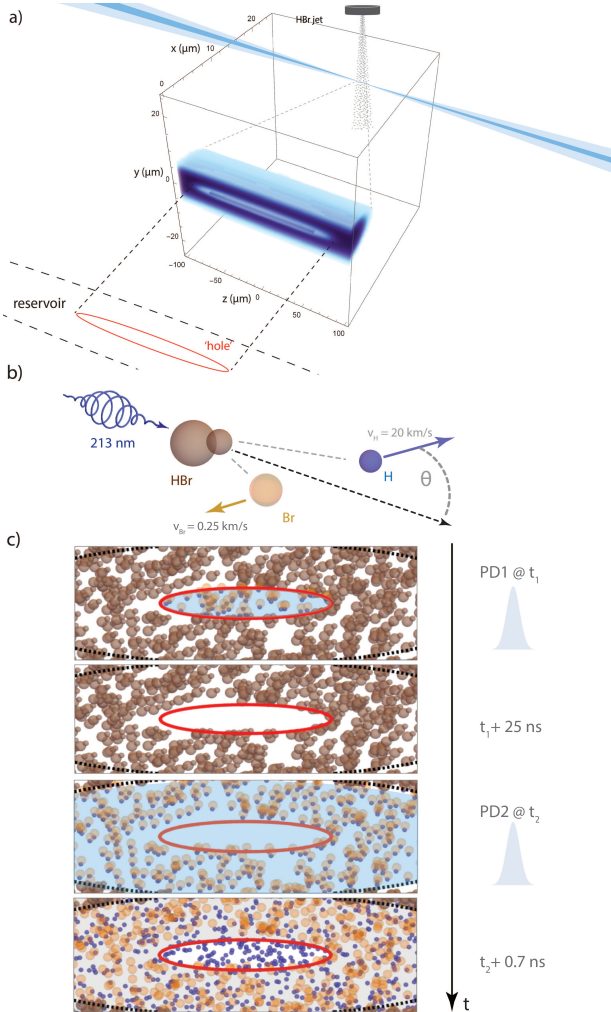


FIG. 1: a) Experimental setup, showing the gas jet and laser beams. b) Velocities associated with the dissociation process. c) The stages of the experiment. (1) complete photodissociation only in area of hole; (2) hole empties of atoms; (3) complete photodissociation in reservoir around hole; (4) hole fills with SPH.

a prolate ellipsoid, with semi-axes a , b and c , which are parallel to x , y , and z axes, respectively. Dissociating HBr at 213 nm inside the hole will result the H atoms acquiring a speed $v_H \approx 20337$ m/s and the Br atoms acquiring a speed $v_{Br} \approx 255$ m/s (Fig.1b). This way, after firing DP1, the H atoms will leave the volume of the hole in a few ps, and subsequently, the Br atoms will also exit in few tens of ns. Note that, in 15 ns, the HBr molecules will have moved less than half a μm towards random directions (in our moving reference frame) due to their thermal motion at $\lesssim 3$ K. After ≈ 25 ns, DP2 can be fired, which will produce fast SPH atoms in the reservoir, which will then rapidly fill the hole after ≈ 0.7 ns (Fig.1c).

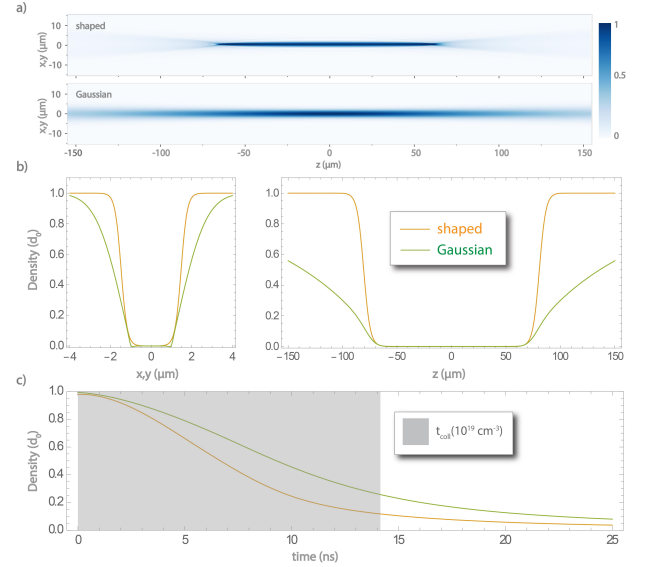


FIG. 2: Two-dimensional intensity maps for the spatially shaped (up) and the Gaussian (down) pulsed beams considered as PD1. b) HBr density in the vicinity of the hole in the x/y (left) and z (right) directions, prepared using the shaped (orange line) or the Gaussian (green line) pulsed beams. c) Density in the hole area as a function of time after firing DP1.

Since the geometric characteristics of the hole and reservoir volumes determine the SPH density and polarization, we consider two experimentally feasible laser beam geometries, with spatial intensity distributions such as the ones shown in Fig.2a. By modulating the spatial spectrum of a Bessel beam [25], we can engineer its intensity profile, achieving a top-hat like distribution along the propagation direction, and a very narrow, Bessel-like distribution in the transverse direction. In the upper part of Fig.2a, we see a two-dimensional intensity map of such a shaped laser beam, while in the lower part that of a conventional Gaussian laser beam with a similar waist ($\approx 2 \mu\text{m}$). In Fig.2b, we see the calculated density distribution in the vicinity of the hole, in the x/y (left) and z (right) directions, created either using the shaped, or the conventional Gaussian laser beam. Such a den-

sity distribution will be created after sufficient time has passed after firing DP1, on the order of a few tens of ns, as shown in Fig.2c. We note that for a number density in the gas-jet around 10^{19} cm^{-3} , only one Br-Br collision is expected to occur for the first 14 ns, a fact that indicates the method's potential for use in high-density experiments.

After $t \gtrsim 15$ ns PD2 is fired. Inside the hole, there are neither H nor Br atoms or HBr molecules. However, in the volume of the reservoir, all HBr molecules will be dissociated. Following dissociation, fast moving SPH atoms move towards all directions, with a large number of them ending up in the volume of the hole. The polarization of these atoms depends on their emission angle: ns laser dissociation of HBr results in narrow velocity distributions for the atomic fragments, which are routinely measured, for example using the VMI technique [26]. For dissociation around 213 nm, the velocity distribution as a function of angle is $I(\theta) = N(1 + \frac{1}{2}P_2(\cos\theta))$, with $P_2(x)$ being the Legendre polynomials of order 2 and N a normalization factor. At the same time, the polarization of the emitted hydrogen atoms depends on θ as $P(\theta) = \cos^2\theta$. In both cases, the angle θ is the apex angle used in spherical coordinates (shown in Fig.1b), i.e. the dissociation laser beams propagate parallel to the z axis with $\theta = 0$. Note that, following dissociation, the polarization of the hydrogen atoms is also modified due to the presence of the nuclear spin ($1/2$ for the proton), via the hyperfine interaction [19]; the polarization beating that results from this interaction is shown in Fig.3a.

In Fig.3b, we see the ratio of the density of the hydrogen atoms entering the hole over the initial density of the HBr molecules in the gas-jet, as a function of time after firing DP2. The orange line corresponds to a shaped beam while the green line shows results using a conventional Gaussian beam. We see that in all cases, the density of the SPH atoms rises fast, reaching close to the initial density of the HBr molecules in the molecular beam at $t \approx 0.2$ ns, and afterwards is gradually reduced.

As hydrogen atoms enter the hole, their polarization is a function of (a) their emission angle and (b) the time due to hyperfine depolarization (shown in Fig.3a). For simplicity, we will refer to the polarization as a function of emission angle as *geometric* polarization (P_G); the total (observable) polarization will be referred to simply as *total* polarization and is the product of P_G and the overall time dependence due to the hyperfine mechanism shown in Fig.3a.

In Fig.3c, we show the values for P_G , for the shaped (orange dashed line) and the Gaussian beams (green dashed line). We see that both these curves originate from a value below 40% (the free-space value), and increase to large values, albeit in different timescales. This polarization increase is to be expected: the hole is shaped as a prolate ellipsoid with its large axis parallel to the laser propagation. Hydrogen atoms with recoil veloci-

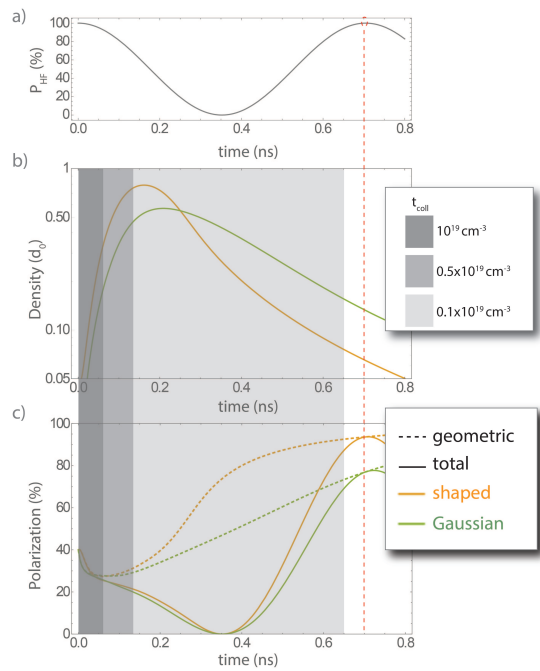


FIG. 3: a) Polarization evolution of the hydrogen electron due to the hyperfine interaction b) Ratio of the density of hydrogen atoms inside the hole over the initial density of the molecular beam, as a function of time after firing DP2. c) P_G (dashed lines) and total polarization (solid lines) of the hydrogen atoms inside the hole as a function of time after firing the PD2.

ties at large angles with respect to the laser propagation axis, and thus the large axis of this ellipsoid, which consequently have poor polarization ($P(\theta \approx \pi/2) \approx 0$), will exit the hole very quickly. On the other hand, highly polarized atoms with recoil velocities at small angles with respect to the laser propagation axis will stay in the hole longer, since they will have to transverse a much larger distance to exit.

The solid lines show the total polarization, i.e. the product of the curve shown in Fig.3a and the dashed lines. We see that the electron polarization is maximized at $t = 0.7$ ns, i.e. the hyperfine period of the electron-proton system. The shaped pulse results in electron polarization close of 93% with a loss of a factor of ≈ 15 in density (shown in Fig.3b), while the Gaussian pulse results in electron polarization around 76%, however at a higher density. Note that all solid curves reach zero at $t = 0.35$ ns (half the hyperfine period for the electron-proton system). At this point all polarization is transferred to the proton nuclear spin, and should be the time to initiate acceleration if high-energy protons are desired. Finally, we note the times for which a single H-H or H-Br collision is expected to occur, for three values of the number density N in the gas jet, using the shaded areas. We see that very few collisions are expected to occur for moderate values of N .

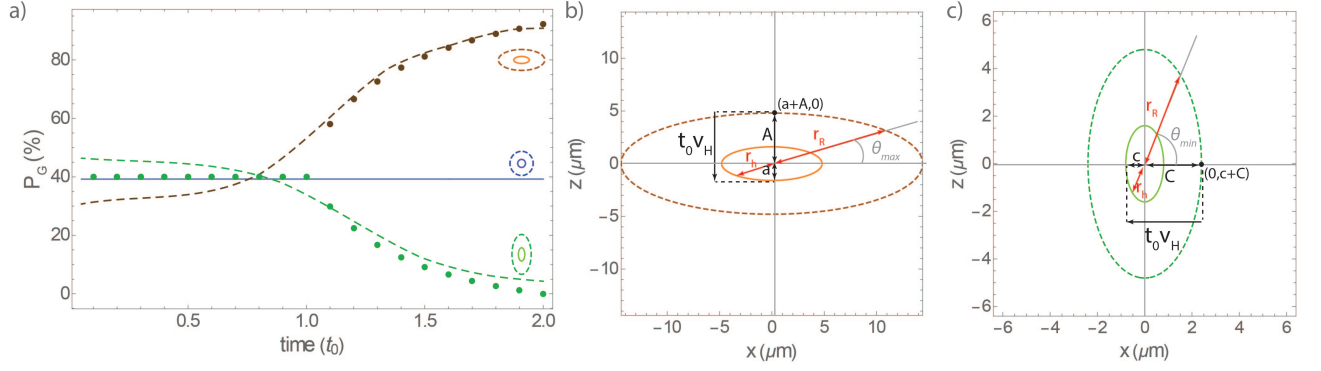


FIG. 4: a) Evolution of P_G inside the hole, for three different geometries for the hole and reservoir, a prolate ellipsoid, an oblate ellipsoid and a sphere. Dashed lines: calculations using pulse parameters similar to the dashed orange curve in Fig.3c. Points: results from Eq.1. b) Integration angles for a given time for a prolate and (c) for an oblate ellipsoid, see text for details.

It is now clear that the geometry of the hole and reservoir is critical for the evolution of P_G : while it does not affect the hyperfine polarization, it defines the value of P_G at the critical time of 0.7 ns. The evolution of P_G can be understood using a qualitative approximating model, which makes use of the integral:

$$P_G = \frac{\int_{\theta_{min}}^{\theta_{max}} P(\theta) I(\theta) \sin\theta d\theta}{\int_{\theta_{min}}^{\theta_{max}} I(\theta) \sin\theta d\theta} \quad (1)$$

where θ_{min} and θ_{max} are the limiting angles for the integration. By setting $\theta_{min} = 0$ and $\theta_{max} = \pi$ for example, one easily obtains the free space value of 40%.

In Fig.4a, we see the evolution of P_G for holes of three different geometries. The brown line corresponds to a prolate ellipsoid, with axes $a = b$, $c = 3a$. The blue line corresponds to a spherical hole while the green line corresponds to a hole with the shape of an oblate ellipsoid ($a = b$, $c = 0.5a$). The widths of the borders of these ellipsoids are similar to the ones used to produce the dashed orange curve shown in Fig.3c. Choosing a spherical geometry for our hole (note that this is impossible to achieve experimentally using lasers), will result in P_G equal to the free-space value of 40% (blue dashed line). In contrast, choosing an elliptical geometry (feasible with lasers) results in P_G different from the free space value: a prolate geometry (orange dashed line) maximizes whereas an oblate geometry (green dashed line) minimizes P_G as time increases.

The brown and green points are values obtained for different choices for θ_{min} and θ_{max} in Eq.1. Let's first discuss the case of a prolate ellipsoid considered in Fig.4b. The red ellipse is a slice of the hole, and the dashed brown a slice of the reservoir, in the xz plane. 'a' and 'A' are either of the small axes of the hole and reservoir ellipsoids. Consider the first quadrant; the complete results can be obtained by reflecting the resulting angles over the x and z axes respectively. In the x direction, the last atoms will exit the ellipse at time $t = t_0 = \frac{a+A}{v_H}$. After this time,

no atoms will be present in the trap coming from this direction, thus their polarization will no longer contribute to the overall geometric polarization inside the hole. In this direction ($\theta = \pi/2$), the polarization is zero (since $P(\theta) = \cos^2\theta$), thus, the overall P_G inside the hole will increase (at the cost of reduced density). At a later time t , more atoms found in the outer limits of the reservoir will be exiting the hole, and in particular those for which $r_h + r_R = t v_H$, via which one can deduce a limiting value for θ_{max} in the integration of Eq.1 ($\theta_{min} = 0$), from which one can obtain the brown points in Fig.4a.

The situation is similar in the case of an oblate ellipsoidal geometry shown in Fig.4c. The light green ellipse is a slice of the hole and the dashed dark green ellipse a slice of the reservoir, in the xz plane. Here, the first atoms leaving the hole are moving in the z direction. Thus, at later times, a similar integration angle can be found, however, now it will be the angle θ_{min} of Eq.1 ($\theta_{max} = \pi/2$), which results in the green points of Fig.4a.

A highly polarized sample of pure SPH can be efficiently produced using spatially shaped pulses at the expense of losing a factor of ≈ 15 with respect to the initial gas jet density. The initial gas density is a parameter which requires experimental investigation. However, if we consider a gas-jet of 3×10^{19} HBr/cm³, we expect a density greater than 10^{18} SPH/cm³ at $t = 0.7$ ns, while staying in a regime of few collisions within the experimental timescales. The energy acquired by the electrons upon laser acceleration is a function of the gas-target density and can be estimated as $E_{max} = m_e c^2 \frac{2\omega_p^2}{\omega_p^2}$ [17], with ω being the laser and ω_P the plasma frequencies, with the latter being $\omega_p = \sqrt{\frac{n_p e^2}{m_e \epsilon_0}}$ where n_p is the plasma density. The length over which the acceleration takes place can be estimated as $l_{acc} = \frac{2\omega_p^2 c}{\omega_p^3}$.

Assuming that total conversion of SPH gas targets into plasma can be achieved by a ps acceleration pulse, we calculate the values for the electron energy and acceleration length shown in Fig.5. We see that for a number

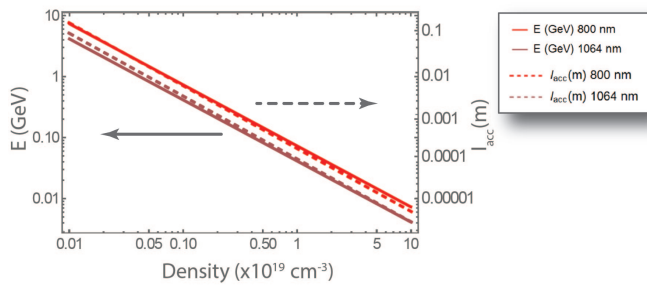


FIG. 5: Energy of accelerated electrons and acceleration length as a function of plasma density, for acceleration laser wavelengths of 800 and 1064 nm.

density of around 10^{18} SPH/cm³ for the isolated SPH atoms, which corresponds to a gas-jet initial density of $\approx 1.5 \times 10^{19}$ HBr/cm³, energies around 1 GeV are predicted, while the acceleration length is comparable to the hole dimensions. We note that these results are estimations considering conventional wakefield acceleration [17]; more advanced acceleration methods utilizing combinations of more than one acceleration pulses [21], or chirped acceleration pulses [27], might generate substantially different results.

We have shown how, by combining the unique optical properties of shaped pulses with the stereodynamics of the photodissociation process, one can prepare an isolated sample of highly polarized SPH atoms, to be used in laser initiated electron acceleration experiments. We have chosen to demonstrate how a sample suitable for conventional wakefield acceleration can be prepared to allow energies well into the GeV regime. Owing to the simplicity of the proposed method and the universality of the photodissociation dynamics, it is straightforward to design similar experiments in a multitude of geometries to fit the needs of particular laser acceleration schemes.

Acknowledgments

TPR acknowledges partial financial support by the Hellenic Foundation for Research and Innovation (HFRI) and the General Secretariat for Research and Technology (GSRT), grant agreement No. HFRI-FM17-3709 (project NUPOL).

* Electronic address: sofdim@uoi.gr

- [1] J. Kessler, in *Advances in atomic, molecular, and optical physics* (Elsevier, 1990), vol. 27, pp. 81–163.
- [2] T. Gay, *Advances in Atomic, Molecular, and Optical Physics* **57**, 157 (2009).
- [3] J. R. Danielson, D. H. E. Dubin, R. G. Greaves, and C. M. Surko, *Rev. Mod. Phys.* **87**, 247 (2015).

- [4] P. J. Schultz and K. G. Lynn, *Rev. Mod. Phys.* **60**, 701 (1988).
- [5] T. Sun, Q. Zhao, K. Xue, Z.-W. Lu, L.-L. Ji, F. Wan, Y. Wang, Y. I. Salamin, and J.-X. Li, *Reviews of Modern Plasma Physics* **6**, 38 (2022).
- [6] B. Barish and J. E. Brau, *International Journal of Modern Physics A* **28**, 1330039 (2013).
- [7] D. Androić, D. S. Armstrong, A. Asaturyan, T. Averett, J. Balewski, K. Bartlett, J. Beaufait, R. S. Beminiwattha, J. Benesch, F. Benmokhtar, et al., *Nature* **557**, 207 (2018).
- [8] B. S. Schlimme, P. Achenbach, C. A. Ayerbe Gayoso, J. C. Bernauer, R. Böhm, D. Bosnar, T. Challand, M. O. Distler, L. Doria, F. Fellenberger, et al., *Phys. Rev. Lett.* **111**, 132504 (2013).
- [9] A. Sokolov and I. Ternov, Chomet and edited by CW Kilmister (American Institute of Physics, New York, 1986) (1986).
- [10] W. von Drachenfels, F. Frommberger, M. Gowin, W. Hillert, M. Hoffmann, and B. Neff, *AIP Conference Proceedings* **675**, 1053 (2003).
- [11] H. Batelaan, A. S. Green, B. A. Hitt, and T. J. Gay, *Phys. Rev. Lett.* **82**, 4216 (1999).
- [12] M. M. Dellweg and C. Müller, *Phys. Rev. Lett.* **118**, 070403 (2017).
- [13] D. T. Pierce, F. Meier, and P. Zürcher, *Applied Physics Letters* **26**, 670 (2008).
- [14] J. Maxson, I. Bazarov, B. Dunham, J. Dobbins, X. Liu, and K. Smolenski, *Review of Scientific Instruments* **85**, 093306 (2014).
- [15] I. Barth and O. Smirnova, *Phys. Rev. A* **88**, 013401 (2013).
- [16] Z. Nie, F. Li, F. Morales, S. Patchkovskii, O. Smirnova, W. An, N. Nambu, D. Matteo, K. A. Marsh, F. Tsung, et al., *Phys. Rev. Lett.* **126**, 054801 (2021).
- [17] T. Tajima and J. M. Dawson, *Physical review letters* **43**, 267 (1979).
- [18] T. P. Rakitzis, P. C. Samartzis, R. L. Loomes, T. N. Kit-sopoulos, A. Brown, G. G. Balint-Kurti, O. S. Vasyutin-skii, and J. A. Beswick, *Science* **300**, 1936 (2003).
- [19] D. Sofikitis, C. S. Kannis, G. K. Boulogiannis, and T. P. Rakitzis, *Phys. Rev. Lett.* **121**, 083001 (2018).
- [20] A. K. Spiliotis, M. Xygkis, M. E. Koutrakis, K. Tazes, G. K. Boulogiannis, C. S. Kannis, G. E. Katsoprinakis, D. Sofikitis, and T. P. Rakitzis, *Light: Science & Applications* **10**, 35 (2021).
- [21] T. Sun, Q. Zhao, F. Wan, Y. I. Salamin, and J.-X. Li, *Physical Review Letters* **132**, 045001 (2024).
- [22] M. Wen, M. Tamburini, and C. H. Keitel, *Phys. Rev. Lett.* **122**, 214801 (2019).
- [23] S. Bohlen, Z. Gong, M. J. Quin, M. Tamburini, and K. Pöder, *Phys. Rev. Res.* **5**, 033205 (2023).
- [24] Y. Wu, L. Ji, X. Geng, Q. Yu, N. Wang, B. Feng, Z. Guo, W. Wang, C. Qin, X. Yan, et al., *New journal of physics* **21**, 073052 (2019).
- [25] T. Čížmár and K. Dholakia, *Optics express* **17**, 15558 (2009).
- [26] T. P. Rakitzis, P. Samartzis, R. Toomes, and T. N. Kit-sopoulos, *The Journal of chemical physics* **121**, 7222 (2004).
- [27] H. S. Ghotra, *Optik* **260**, 169080 (2022).